Diffuse interseismic deformation across the Pacific–North America plate boundary

Shimon Wdowinski   Division of Marine Geology and Geophysics, University of Miami, 4600 Rickenbacker Causeway, Miami, Florida 33149-1098, USA

Bridget Smith-Konter
Yehuda Bock
David Sandwell   Cecil H. and Ida M. Green Institute of Geophysics and Planetary Physics, Scripps Institution of Oceanography, La Jolla, California 92093-0210, USA

ABSTRACT

Crustal movements and deformation within the diffuse Pacific–North America (Pa-NA) plate boundary are dominated by the right-lateral motion between the two plates. By using the Pa-NA pole of rotation (PoR) spherical coordinate system, we decompose observed crustal movements into parallel and normal components to the Pa-NA plate motion. We transformed the 840 velocity vectors of the Southern California Earthquake Center (SCEC) 3.0 velocity field into the Pa-NA PoR system in order to characterize the interseismic velocity across the plate boundary. Our results show that despite the very different deformation styles occurring across the San Andreas fault, the fault trace follows the half plate motion contour. Deviation occurs in the southern section, where the half motion contour correlates with the San Jacinto and Imperial fault segments. Our analysis yields interesting asymmetric patterns in both parallel and normal components. The parallel component shows asymmetrical velocity gradients across the San Andreas fault, and the normal component indicates compression southwest of the Big Bend, but not northeastward. The observations are compared with viscoelastic modeling results, which show a similar velocity field. The main disagreements between the observations and the model are in a narrow band along the San Andreas fault and in the Mojave block, suggesting that crustal heterogeneities and additional unmodeled fault segments should be considered in future models.

Keywords: crustal deformation, plate motion, San Andreas fault, viscoelastic model, deformation asymmetry.

INTRODUCTION

The relative motion between the Pacific and North America plates primarily occurs along the San Andreas fault system, but some significant deformation occurs along other tectonic elements, such as along the Eastern California shear zone and across the Basin and Range. An insight to the plate boundary deformation can be obtained from the increased number of geodetic observations collected over the past three decades by precise geodetic instrumentation. Deformation varies both in space and time, reflecting a complex crustal structure and simultaneous response to several forces by several deformation mechanisms. The one largely time-independent component is the interseismic deformation, occurring between large earthquakes. It represents mainly elastic crustal strain accumulation between large earthquakes, but may also include long-term viscous relaxation of the uppermost mantle in response to large earthquakes.

In recent years, results of various geodetic networks in the western United States have been integrated into a single interseismic velocity field (e.g., Shen et al., 1997, 2003; Bennett et al., 1999), most often with respect to a stable North America reference frame (RF). The Southern California Earthquake Center (SCEC) velocity crustal motion models (Shen et al., 1997, 2003) were used to quantitatively estimate horizontal velocity gradient and strain rate tensor fields across the Pacific–North America (Pa-NA) diffuse plate boundary (Jackson et al., 1997; Shen-Tu et al., 1999; Kreemer et al., 2003), to constrain slip rate and locking depth along major fault segments (Wdowinski et al., 2001; Smith and Sandwell, 2003; McCaffrey, 2005; Bos and Spakman, 2005; Meade and Hager, 2005), and to detect active faults in southern California (Wdowinski et al., 2001).

In this study we use the SCEC 3.0 crustal motion model (Shen et al., 2003) to characterize the interseismic velocity in southern California. We find that the deformation's main driving process, the relative motion between the Pacific and North America plates, also provides the best RF for analyzing the geodetic data. By transforming the SCEC 3.0 velocity field to the Pa-NA pole of rotation (PoR) spherical coordinate system, we identify important relations between the geodetic velocities and geographic location of the active fault segments. We also detect symmetric and asymmetric components of the velocity field, reflecting inhomogeneous crustal structure across the San Andreas fault system. Comparing our observations to a detailed fault model enables us to explain many of the observed patterns, as well as identify anomalous regions that require modifications of the model.
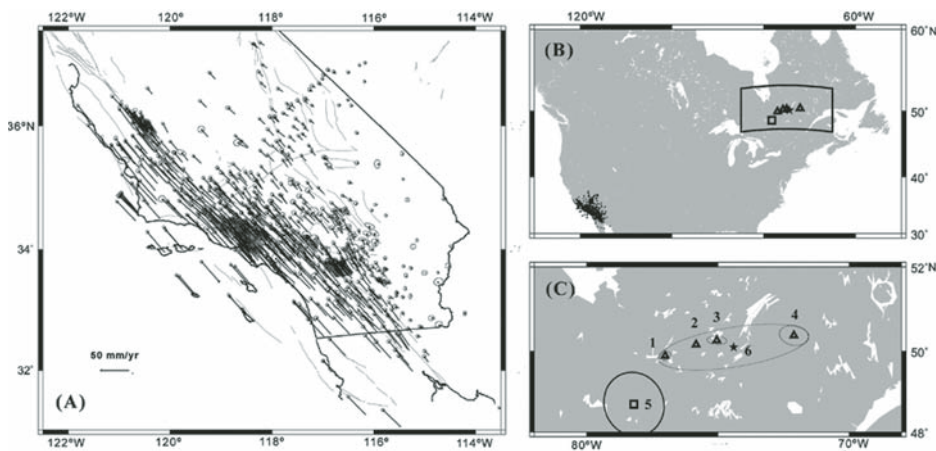
SCEC 3.0 VELOCITY FIELD

The SCEC crustal motion model version 3.0 (Shen et al., 2003) consists of 840 velocity vectors, covering the entire southern California region. The velocity vectors were calculated from trilateration, very long baseline interferometry, and global positioning system (GPS) measurements collected in Southern California since 1970. The spatial coverage is not uniform. It is dense along the trace of the San Andreas fault, the Los Angeles Basin, and the Landers epicentral region and somewhat sparse in the less seismically active areas. Of the 840 vectors, we omitted 14, which are reported as possible problem sites.

The SCEC velocity vectors are oriented to the northwest along the expected direction of Pacific plate motion with respect to North America (Fig. 1A) and roughly parallel to the orientation of the San Andreas fault system. They also show a gradual southwestward magnitude increase perpendicular to the general shape of the plate boundary, reflecting the velocity transition from stable North America plate (zero velocity) to the full Pacific plate motion.

POLE OF ROTATION ANALYSIS

The best estimate of the long-term relative rotation vector for the Pacific and North America plates is the NUVEL-1A plate model obtained from marine magnetic anomalies and earthquake data (DeMets et al., 1994). Shen-Tu et al. (1999) and Wdowinski et al. (2001) noticed a 4°–6° misalignment between the NUVEL-1A predicted motion and the SCEC 2.0 velocity field (Shen et al., 1997), suggesting that the NUVEL-1A pole is not consistent with geodetic observations in western North America. Because the actual pole location plays an important role in our analysis, we calculate an average PoR based on four recent GPS-determined estimates (Table DR1 in GSA Data Repository item DR1[1]). Although each of the four studies reports very high accuracy levels, as shown by their very small uncertainty ellipses, their locations are spread over a wide area (Fig. 1C).

---

[1]GSA Data Repository item 2007077, DR1 (uncertainty analysis of the average PoR velocity field) and DR2 (viscoelastic modeling), is available online at www.geosociety.org/pubs/ft2007.htm, or on request from editing@geosociety.org or Documents Secretary, GSA, P.O. Box 9140, Boulder, CO 80301, USA.

Figure 1. A: Southern California Earthquake Center 3.0 velocity field in stable North America reference frame. B: Geographic locations of recent Pacific–North America pole of rotation estimates with respect to location of velocity observations (black dots). C: Pole estimate locations and their 95% confidence ellipses. Different estimates are provided in Table DR1 (see footnote 1).

We transform the SCEC 3.0 crustal motion model to our calculated (average) Pa-NA PoR spherical coordinate system (Fig. 2A). A statistical analysis of the average velocity vectors, and their uncertainties, is presented in DR1 (see footnote 1). The transformation decomposes the velocity vectors into parallel and normal plate motion components. The parallel component follows the direction of small circles about the PoR (vertical lines in Fig. 2A). Because the magnitude of plate motion increases with distance from the pole, we normalize the velocity vectors by our full plate motion rate estimate (0.765°/m.y.). We present the parallel component in the half plate motion RF, which constrains the dimensionless velocity in the range of ±1/2; −1/2 represents stable North America and +1/2 is stable Pacific. The plate motion normal component follows the direction of great circles about the PoR. The normalized value of the normal component is in the range ±0.15, which is roughly equivalent to ±3 mm/yr.

RESULTS

The normalized SCEC 3.0 velocity field in the PoR coordinate system (Fig. 2A) shows the velocity transition across the Pa-NA plate boundary. The transition between negative and positive parallel velocity (zero velocity contour) occurs, in general, along the trace of the San Andreas fault from the Parkfield segment in the north (Fig. 2B) to the southern section of the Big Bend. This observation indicates that the San Andreas fault is the boundary between the Pacific and North America plates. We find this surprising because the deformation styles on both sides of the San Andreas fault are very different. East of the fault, the deformation is characterized by block rotations and formation of a large fault zone (Eastern California shear zone), whereas west of the fault, the deformation is more diffusive. South of the Big Bend, the zero contour does not follow the

San Andreas fault segment, but rather is located just east of the San Jacinto fault (SJF) segment (Fig. 2C). Farther south the zero contour follows the Imperial and Cerro Prieto fault segments.

As geodetic velocity vectors represent a relative motion, our choice of RF is critical. Many studies use stable North America RF to present velocity variation across the Pa-NA plate boundary (e.g., Fig. 1). However, Shen et al. (2003) found that this approach masks the finer details of the velocity variations, and presented the SCEC vectors in the Pa-NA half plate motion reference. Our velocity analysis also demonstrates that the half plate motion is a very useful reference. However, in order to eliminate further bias that can arise from the choice of RF, we decouple the two velocity components. We use a triangulation and contouring algorithm (generic mapping tool contour; Wessel and Smith, 1991) to plot the lateral variations of each velocity component. The results presented in Figures 3A and 3D show our preferred analysis; data points with 1σ uncertainty level greater than the velocity component are omitted from the analysis. The same analysis with a 2σ criterion eliminates too many data points, although it produces very similar results.

The analysis of the parallel component (Fig. 3A) reveals several interesting observations. First, the geographic location of the half plate motion (zero contour) follows the geographic location of the San Andreas, San Jacinto, Imperial, and Cerro Prieto fault segments. The parallel component also shows an asymmetrical velocity gradient across the San Andreas fault. North of the Big Bend, high gradients are located west of the fault, whereas south of the Big Bend the high gradients are located east of the fault. The parallel component also indicates that the plate boundary is very wide in the north, across the San Andreas fault and the Eastern California shear zone segments, and becomes narrower south of the Big Bend.

The analysis of the normal component (Fig. 3D) also reveals interesting features. The most noticeable pattern is the lack of symmetry across the San Andreas fault system. In the central section of the San Andreas fault, along the Big Bend segment, the area located west of the fault shows a significant westward motion (red in Fig. 3D), whereas east of the fault the normal motion is negligible. This asymmetry across the Big Bend can also be seen in Figure 2A, which shows westward rotation of the velocity field west of the fault and southward velocity east of the fault. The normal component map (Fig. 3D) also shows localized areas with significant eastward (blue) or westward (red) normal velocity. The red anomaly north of the Garlock fault is associated with a lower number of observations and may be contaminated by oilfield operations near Bakersfield. The northern blue anomaly is also located near oilfields (Coalinga) and may reflect nontectonic movements. However, some of the localized normal signal is tectonic and is explained by our model.

VISCOELASTIC MODELING

In order to explain the observed patterns of the transformed velocity field (Figs. 3A, 3D), we calculated an expected velocity field using elastic and viscoelastic models. The model is based on the work of Smith and Sandwell (2006) and accounts for the three dominant processes governing interseismic crustal movements: elastic strain accumulation, elastic coseismic displacements, and postseismic viscous relaxation of the mantle beneath. We ran a series of models with several fault segment configurations and slip rate estimates; here we present the results of the best-fit model (Figs. 3B, 3E). A more detailed description of the model is presented in Data Repository item DR2 (see footnote 1).

COMPARISON BETWEEN OBSERVATIONS AND MODEL

We compare both parallel and normal components of the SCEC 3.0 velocity field to the expected crustal movements derived from a viscoelastic model (Figs. 3C, 3F). The fit level of the parallel component (weighted root mean square [rms] of the residuals) is 1.98 mm/yr and that of the normal component is 1.80 mm/yr. The rms values are 1.5 times larger than the mean uncertainties (1.2 mm/yr for components), but reflect only 4%–5% of the Pa-NA full plate motion (50 mm/yr). However, locally the misfit can reach 5–8 mm/yr, which is 10%–16% of the full plate motion. Some of the misfit can be attributed to nontectonic processes, such as oilfield operations. Nevertheless, most of the misfit reflects unmodeled fault segments, unaccounted earthquakes, uncertainties in slip rate and locking depth values, and crustal heterogeneities.

Although the overall fit of the parallel component is good, we notice some second-order
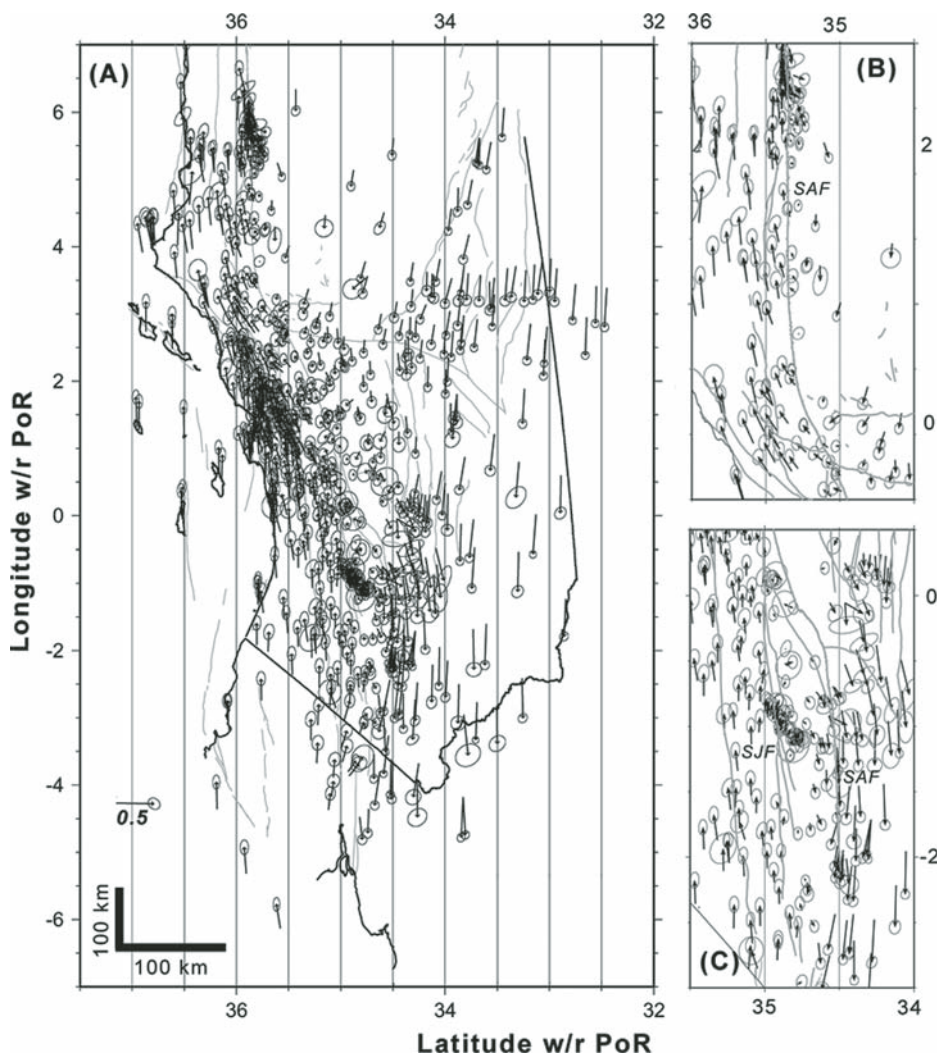
Figure 2. A: Southern California Earthquake Center velocity field version 3.0 for Southern California in the Pacific–North America pole of rotation reference frame. Velocities are normalized by Pacific–North America full plate motion and presented with half of plate motion subtracted. In order to show many details, we chose 1:2.5 aspect ratios between latitudinal and longitudinal coordinates (see 100 km scales). Vertical lines are grid lines representing small circles about pole of rotation (PoR). B: San Andreas fault (SAF) Parkfield-Carrizo segments showing that zero velocity occurs along trace of San Andreas fault. C: Southern San Andreas fault and San Jacinto fault (SJF) segments showing that zero velocity occurs just east of trace of SJF.

ern San Andreas is possibly due to postseismic deformation from the 1999 Hector Mine earthquake. Purely elastic models (not containing postseismic effects of the Hector Mine earthquake) fail to produce an eastward-trending zone of deformation similar to that observed in the data. Furthermore, the normal residuals reveal one particular region of misfit north of the Garlock fault, possibly due to the omission of normal faulting in the Sierra Nevada.

DISCUSSION AND CONCLUSIONS

The Pa-NA PoR spherical coordinate system is the natural RF for analyzing and modeling crustal movements and deformation within the wide diffuse Pa-NA plate boundary because it decomposes the velocity vectors and uncertainties into parallel and normal components. The normal component is overall very small (0–4 mm/yr), but locally reaches 8 mm/yr. The choice of RF is a key issue in tectonic interpretation of geodetic observations. Velocity vectors plotted in the commonly used stable North America RF, or the stable Pacific RF, nicely show the gradual transition of the parallel component between the two plates, but mask variations in the normal component. The half plate motion RF suggested by Shen et al. (2003) is sensitive to the normal component along the San Andreas fault system, but not in the far field. The best way to characterize changes in velocity orientation throughout the deforming plate boundary is to separately evaluate the parallel and normal components, as in this study. By separating the two components, the deviation of the velocity vectors from the expected parallel motion can be evaluated in an objective way.

Our PoR analysis highlights the asymmetric patterns across the San Andreas fault system in both parallel and normal components. The parallel component shows asymmetric velocity gradients across the San Andreas fault system, especially along the northern segments (Fig. 3A), whereas the normal component shows a significant westward motion west of the Big Bend (red in Fig. 3D), but not a comparable normal motion east of the San Andreas fault. Our modeling results yield a similar asymmetric pattern in the normal component (Fig. 3E), but fail to predict the asymmetry in the parallel component (Fig. 3B). The residual parallel component shows 5–8 mm/yr of unaccounted motion along both sides of the San Andreas fault (Fig. 3C). The misfit in parallel component indicates that the asymmetrical velocity gradients across the San Andreas fault cannot be explained by the fault segment geometry and the assumed slip rates. This asymmetry was noted by Schmalzle et al. (2006) and was explained as a result of heterogeneous crustal strength across the San Andreas fault. High-resolution imaging of the Parkfield and Bear Valley sections of the San Andreas fault with seismic head waves that refract along material interfaces also reveals

misfits, which are emphasized in the residual map by means of the condensed color scale (Fig. 3C). The main differences between the observations and the model are located in a narrow band along the San Andreas fault, in the Mojave block, and in a localized spot along the Eastern California shear zone. A large region of positive misfit can be observed along the San Bernardino Mountains region, extending into the Eastern California shear zone. This feature is visible in both viscoelastic and elastic versions of the model, although comparatively, it is suppressed in the viscoelastic model. Two explanations are possible for this anomaly: (1) additional slip along faults in the Eastern California shear zone is required, or (2) reduction of slip rate on the San Bernardino segment is necessary. We plan to further investigate the nature

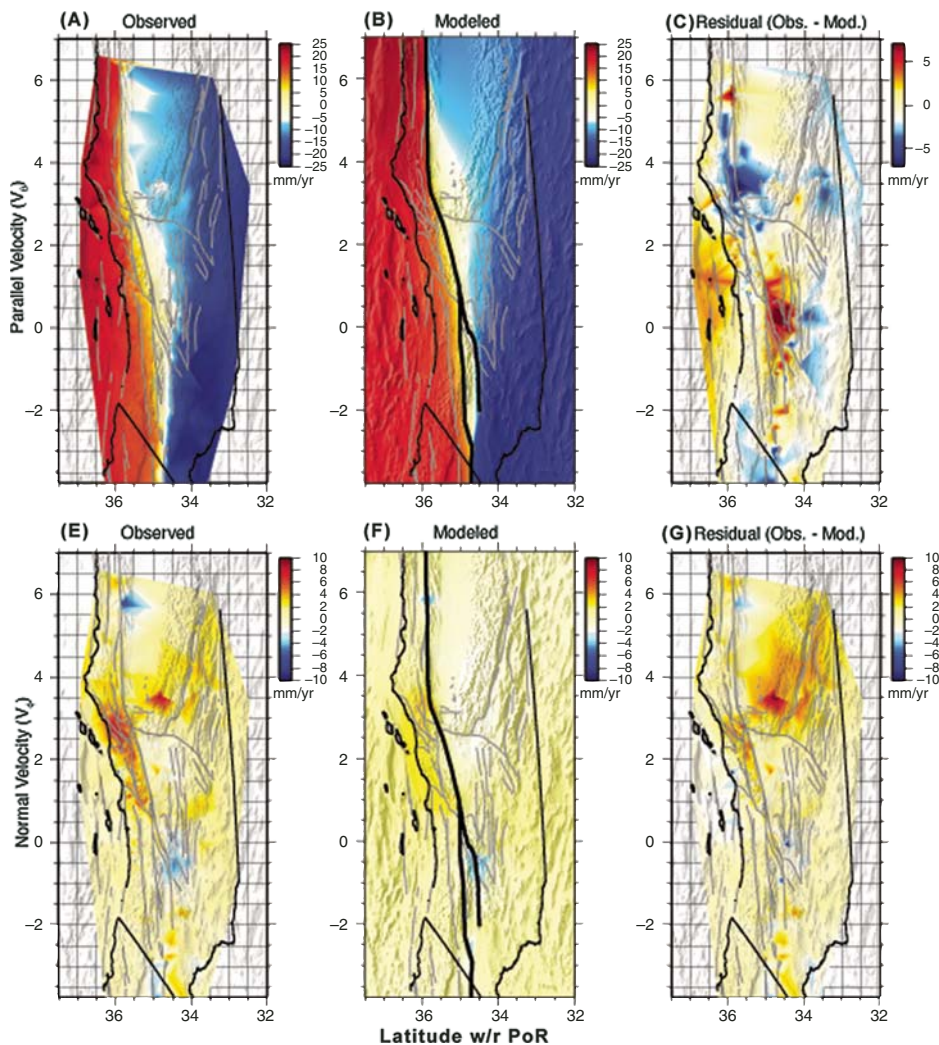of this anomaly as we incorporate additional contributions of faulting into the model.

The overall fit of the modeled normal velocity component is in good agreement with the data over the entire span of our study region (Fig. 3F). Both observations and model reveal a westward-trending zone west of the Mojave segment and the Big Bend; however, the amplitude of the feature produced by the model is slightly lower. This feature is attributed to the westward-bending geometry of the fault system. Furthermore, both data and model indicate zones of eastward-trending deformation south of Parkfield and along the southern San Andreas. The modeled east-trending region near Parkfield is due to an abrupt transition from a locked fault (10.2 km) to a nearly (unlocked) creeping fault. Alternatively, the noted zone along the south-

Figure 3. Parallel and normal components of observed, modeled, and residual velocity fields. Comparison shows small parallel residuals, mainly along trace of San Andreas fault (C), indicating good agreement between observed (A) and modeled (B) fields. North-oriented velocity is taken to be positive for parallel component. Also note that smaller scale is used in residual map (C). Normal residual (F) indicates very minor differences between observed (D) and modeled (E) fields. West-oriented velocity is taken to be positive for normal component. PoR—pole of rotation.

significant contrast of material properties across the fault (McGuire and Ben-Zion, 2005).

The comparison between the observed and modeled velocity fields shows an overall very good agreement, suggesting that most of the observed interseismic motion can be explained by elastic strain accumulation of the crust and postseismic viscous relaxation of the mantle beneath. The reasonable fit along the San Andreas fault (zero contour) suggests that the San Andreas fault marks the Pa-NA plate boundary because the motion below the locked seismogenic crust is localized along a plane that follows the San Andreas fault. The main disagreements between the observation and the model are located in a narrow band along the San Andreas fault and in the Mojave block, suggesting that crustal heterogeneities and additional unmodeled fault segments should be considered in future models.

REFERENCES CITED

Bennett, R.A., Davis, J.L., and Wernicke, B.P., 1999, Present-day pattern of Cordilleran deformation in the western United States: Geology, v. 27, p. 371–374, doi: 10.1130/0091-7613(1999)027<0371:PDPOCD>2.3.CO;2.

Bos, A.G., and Spakman, W., 2005, Kinematics of the southwestern US deformation zone inferred from GPS motion data: Journal of Geophysical Research–Solid Earth, v. 110, doi: 10.1029/2003JB002742.

DeMets, C., Gordon, R.G., Argus, D.F., and Stein, S., 1994, Effect of recent revisions to the geomagnetic reversal time-scale on estimates of current plate motions: Geophysical Research Letters, v. 21, p. 2191–2194, doi: 10.1029/94GL02118.

Jackson, D.D., Shen, Z.K., Potter, D., Ge, X.B., and Sung, L.Y., 1997, Southern California deformation: Science, v. 277, p. 1621–1622, doi: 10.1126/science.277.5332.1621.

Kreemer, C., Holt, W.E., and Haines, A.J., 2003, An integrated global model of present-day plate motions and plate boundary deformation: Geophysical Journal International, v. 154, p. 8–34, doi: 10.1046/j.1365-246X.2003.01917.x.

McCaffrey, R., 2005, Block kinematics of the Pacific–North America plate boundary in the southwestern US from inversion of GPS, seismological, and geologic data: Journal of Geophysical Research, vol. 110, B07401, doi: 10.1029/2004JB003307.

McGuire, J., and Ben-Zion, Y., 2005, High-resolution imaging of the Bear Valley section of the San Andreas fault at seismogenic depths with fault-zone head waves and relocated seismicity: Geophysical Journal International, v. 163, p. 152-164, doi: 10.1111/j.1365-246X.2005.02703.x.

Meade, B.J., and Hager, B.H., 2005, Block models of crustal motion in southern California constrained by GPS measurements: Journal of Geophysical Research–Solid Earth, v. 110, doi: 10.1029/2004JB003209.

Schmalzle, G.M., Dixon, T., Malservisi, R., and Govers, R., 2006, Strain accumulation across the Carrizo segment of the San Andreas Fault, California: Impact of laterally varying crustal properties: Journal of Geophysical Research, B, Solid Earth and Planets, v. 111, B05403, doi: 10.1029/2005JB003843.

Shen-Tu, B.M., Holt, W.E., and Haines, A.J., 1999, Deformation kinematics in the western United States determined from Quaternary fault slip rates and recent geodetic data: Journal of Geophysical Research–Solid Earth, v. 104, p. 28,927–28,955, doi: 10.1029/1999JB900293.

Shen, Z.-K., Dong, D., Herring, T., Hudnut, K., Jackson, D., King, R.S.M., and Sung, L., 1997, Geodetic measurements of southern California crustal deformation: Eos (Transactions, American Geophysical Union), v. 78, p. 477, 482.

Shen, Z.-K., Agnew, D.C., King, R.W., Dong, D., Herring, T.A., Wang, M., Johnson, H., Anderson, G., Nikolaidis, R., Domselaar, M.V., Hudnut, K.W., and Jackson, D.D., 2003, The SCEC crustal motion map, Version 3.0: http://epicenter.usc.edu/cmm3. (December, 2006)

Smith, B., and Sandwell, D., 2003, Coulomb stress accumulation along the San Andreas Fault system: Journal of Geophysical Research–Solid Earth, v. 108, doi: 10.1029/2002JB002136.

Smith, B.R., and Sandwell, D.T., 2006, A model of the earthquake cycle along the San Andreas Fault System for the past 1000 years: Journal of Geophysical Research, v. 111, doi: 10.1029/2005JB003703.

Wdowinski, S., Sudman, Y., and Bock, Y., 2001, Geodetic detection of active faults in S. California: Geophysical Research Letters, v. 28, p. 2321–2324, doi: 10.1029/2000GL012637.

Wessel, P., and Smith, W.H.F., 1991, Free software helps map and display data: Eos (Transactions, American Geophysical Union), v. 72, p. 441, doi: 10.1029/90EO00319.

Printed in USA